

Do Unstable Systems Have Amplification and Phase Shift?

KHALED F. ALJANAIDEH, JAMES R. FORBES, and DENNIS S. BERNSTEIN

Control textbooks sometimes give the impression that amplification and phase shift are properties confined to asymptotically stable systems. For example, [1, p. 400] states that “Any system with a pole in the RHP is unstable; hence it would be impossible to determine its frequency response experimentally because the system would never reach a steady-state sinusoidal response for a sinusoidal input.” This statement is correct in reference to an unstable plant operating in open loop but does not consider the case of an unstable plant operating inside a stabilized closed loop.

The goal of this article is to investigate whether or not an unstable plant in a stabilized closed loop has amplification and phase shift in the sense of the harmonic steady-state response of an asymptotically stable system. If this is indeed the case, then the “frequency response” of the unstable plant, which contributes to the Nyquist plot of the loop transfer function, can be viewed as having the same *physical* meaning as the frequency response of an asymptotically stable system. This is, perhaps, surprising since the same harmonic inputs to the plant *without* the benefit of the stabilizing loop would inevitably lead to an unbounded, and thus nonharmonic, response, regardless of how precisely the initial condition could be specified. The fact that an unstable plant operating inside a stabilized loop can exhibit the same kind of harmonic steady-state response as an asymptotically stable plant serves to emphasize the “miracle” of feedback stabilization (see “The Miracle of Feedback Stabilization”). Moreover, this result may be useful for closed-loop identification of the frequency response of unstable systems.

AMPLIFICATION AND PHASE SHIFT OF ASYMPTOTICALLY STABLE SYSTEMS

The following result characterizes the response of an asymptotically stable linear, time-invariant system to a harmonic input.

Theorem 1 [2]

For $t \geq 0$, consider the linear, time-invariant system

$$\dot{x}(t) = Ax(t) + Bu(t), \quad (1)$$

$$y(t) = Cx(t), \quad (2)$$

where $A \in \mathbb{R}^{n \times n}$ is asymptotically stable, $B \in \mathbb{R}^{n \times 1}$, $C \in \mathbb{R}^{1 \times n}$, and $x(0)$ represents the initial state. Let $u(t) = \operatorname{Re} u_0 e^{j\omega t} = A_u \sin(\omega t + \phi)$, where $u_0 \triangleq -A_u j e^{j\phi} \in \mathbb{C}$, and A_u , ϕ , and ω are real numbers. Then,

$$y(t) = y_{\text{trans}}(t) + y_{\text{hss}}(t), \quad (3)$$

where

$$y_{\text{trans}}(t) \triangleq Ce^{tA}x(0) - \operatorname{Re} [(j\omega I - A)^{-1}Bu_0], \quad (4)$$

$$y_{\text{hss}}(t) \triangleq MA_u \sin(\omega t + \phi + \theta), \\ M \triangleq |G(j\omega)|, \theta \triangleq \angle G(j\omega),$$

and

$$G(s) \triangleq C(sI - A)^{-1}B. \quad (5)$$

The signals y_{trans} and y_{hss} are the transient and harmonic steady-state components of the output, respectively. It follows from (5) that y_{hss} is a harmonic signal with the same frequency as u . Moreover, $|G(j\omega)|$ is the amplification of y_{hss} relative to u , and $\angle G(j\omega)$ is the phase shift of y_{hss} relative to u . The plot of $|G(j\omega)|$ and $\angle G(j\omega)$ versus ω is the Bode plot.

It follows from (4) that

$$\lim_{t \rightarrow \infty} y_{\text{trans}}(t) = 0 \quad (6)$$

and

$$\lim_{t \rightarrow \infty} [y(t) - y_{\text{hss}}(t)] = 0. \quad (7)$$

If, in addition,

$$x(0) = \operatorname{Re} [(j\omega I - A)^{-1}Bu_0], \quad (8)$$

then $y_{\text{trans}}(t) = 0$ for all $t \geq 0$, and thus $y(t) = y_{\text{hss}}(t)$ for all $t \geq 0$. If A is not asymptotically stable, then y_{trans} may not converge to zero.

Figure 1 illustrates the relationship between the phase shift $\angle G(j\omega)$ and the input-output map formed by plotting the normalized amplitudes $(1/MA_u)y_{\text{hss}}$ and $(1/A_u)u$. As shown in Figure 1, the input-output map may be a line segment, a circle, or an ellipse. The phase angle $\angle G(j\omega)$

The Miracle of Feedback Stabilization

Stabilization is explained in various ways, for example, in terms of pole movement or Lyapunov functions. However, these mathematical explanations tend to overlook the fact that stabilization requires very special inputs to drive the state of a system to zero.

To explain this point of view, first consider an unstable plant operating inside a stabilizing closed loop. We then record the state at a given time, which serves as the initial condition, along with the subsequent sequence of inputs. This sequence of inputs is then applied to the plant with the recorded initial condition to determine whether the open-loop plant response matches the response of the plant inside the closed loop. A discrete-time feedback system is used to avoid discretization errors that may arise due to sampling continuous-time signals.

Example S1

Consider the closed-loop system consisting of the discrete-time unstable plant

$$G(z) = \frac{1}{(z-1.1)(z-0.5)}, \quad (\text{S1})$$

the discrete-time controller

$$C(z) = \frac{0.6z-0.4}{z-0.3}, \quad (\text{S2})$$

and unity feedback. The closed-loop system is asymptotically stable with closed-loop poles $0.7269, 0.5866 \pm j0.6582$. For $r(k) = \sin(0.01k)$, simulate the closed-loop system and record the input of G for $0 \leq k \leq 1000$ steps. Figure S1 shows the input and the output of G for this case, defined as u_1 and y_1 , respectively. Then rerun the exact same simulation, where the plant is in closed loop, using the recorded sequence of inputs for $0 \leq k \leq 400$ steps. At $k = 400$ steps. The simulation is frozen, and the internal state of G is recorded. The recorded sequence of inputs is then applied to the plant in open loop for

$400 \leq k \leq 1000$ given the recorded initial condition. Figure S1 shows the input and output of G for this case defined as u_2 and y_2 , respectively, where y_2 diverges quickly after $k = 400$ steps.

Despite this attempt to reapply the same sequence of inputs from the same initial condition, the open-loop response of the plant is unbounded. This example shows that feedback stabilization is indeed quite remarkable—if not miraculous. ■

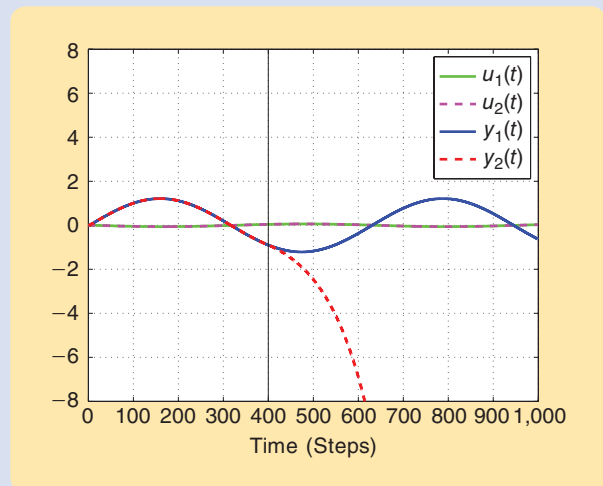


FIGURE S1 Plots of the input u_1 and output y_1 of the closed-loop system consisting of (S1) and (S2), where $r(k) = \sin(0.01k)$, $0 \leq k \leq 1000$ steps. The $u_1(k)$ is recorded for $0 \leq k \leq 1000$ steps and the exact same simulation rerun using the recorded sequence of inputs for $0 \leq k \leq 400$ steps. At time $k = 400$ steps, the simulation is frozen and the internal state of G recorded. Then, the recorded sequence of inputs is applied to the plant in open loop for $400 \leq k \leq 1000$ steps given the recorded initial condition. The input u_2 and output y_2 for this latter case are shown. Note that despite the attempt to reapply the same sequence of inputs from the same initial condition, y_2 diverges quickly after $k = 400$ steps.

can be determined from the input–output maps shown in Figure 1 by using the slope of the semimajor axis of the ellipse or the line segment, which can be either 1 or -1 , the orientation of the plot, and the eccentricity of the ellipse. For details, see “Harmonic Steady-State Phase Shift and the Eccentricity of Ellipsoidal Input–Output Maps.”

In the special case where the input–output map is a line segment, $\angle G(j\omega)$ is zero if the slope of the line segment is 1 and 180° if the slope of the line segment is -1 . If the input–output map is a circle, then $\angle G(j\omega)$ is 90° if the orientation is clockwise and -90° if the orientation is counterclockwise. If the input–output map is an ellipse, then the slope of the semimajor axis of the ellipse, the orientation of the plot, and the eccentricity of the ellipse are needed to determine $\angle G(j\omega)$. Note that, if the slope of the semimajor axis of the ellipse is one, then $\angle G(j\omega) \in (-90, 90)^\circ$, whereas, if the slope of the semimajor axis of

the ellipse is -1 , then, either $\angle G(j\omega) \in (-180, -90)^\circ$ or $\angle G(j\omega) \in (90, 180)^\circ$. Moreover, if the orientation of the input–output map is clockwise, then $\angle G(j\omega) \in (0, 180)^\circ$ where, if the orientation of the input–output map is counterclockwise, then $\angle G(j\omega) \in (-180, 0)^\circ$. The input–output map in each subplot in Figure 1 is a Lissajous figure [3].

The following example illustrates Theorem 1.

Example 1

Consider the asymptotically stable plant

$$G(s) = \frac{1}{s+1} \quad (9)$$

with $u(t) = 3 \sin(t)$. It follows from (5) that

$$\begin{aligned} y_{\text{hss}}(t) &= 3 |G(1j)| \sin(t + \angle G(1j)) \\ &= \frac{3}{\sqrt{2}} \sin\left(t - \frac{\pi}{4}\right), \end{aligned} \quad (10)$$

Harmonic Steady-State Phase Shift and the Eccentricity of Ellipsoidal Input–Output Maps

The input–output map formed by plotting the normalized sinusoidal input versus the normalized harmonic steady-state output of a linear time-invariant system may be a line segment, a circle, or an ellipse (see Figure 1). The phase shift associated with a line segment is zero if the slope of the line segment one and 180° if the slope of the line segment is one. The phase shift associated with a circle is 90° if the orientation of the plot is clockwise and -90° if the orientation of the plot is counterclockwise. If the input–output map is an ellipse, the slope of the semimajor axis of the ellipse and the orientation of the plot determine the quadrant in which the relative phase shift lies, but the value of the relative phase shift is determined by the eccentricity of the ellipse.

Let $\sin(\omega t)$ be the normalized input and $\sin(\omega t + \theta)$ be the normalized harmonic steady-state output of a linear time-invariant system, where $\theta \in (-180, 180]$ is the phase shift. Note that

$$\begin{aligned} \sin^2(\omega t + \theta) &= (\cos \theta \sin(\omega t) + \sin \theta \cos(\omega t))^2 \\ &= \cos^2 \theta \sin^2(\omega t) + \sin^2 \theta \cos^2(\omega t) \\ &\quad + 2 \cos \theta \sin \theta \sin(\omega t) \cos(\omega t) \\ &= \cos^2 \theta \sin^2(\omega t) + \sin^2 \theta (1 - \sin^2(\omega t)) \\ &\quad + 2 \cos \theta \sin \theta \sin(\omega t) \cos(\omega t) \\ &= (\cos^2 \theta - \sin^2 \theta) \sin^2(\omega t) + \sin^2 \theta \\ &\quad + 2 \cos \theta \sin \theta \sin(\omega t) \cos(\omega t) \end{aligned} \quad (S3)$$

and

$$\begin{aligned} \cos \theta \sin(\omega t) \sin(\omega t + \theta) &= \cos \theta \sin(\omega t) (\cos \theta \sin(\omega t) \\ &\quad + \sin \theta \cos(\omega t)) \\ &= \cos^2 \theta \sin^2(\omega t) \\ &\quad + \cos \theta \sin \theta \sin(\omega t) \cos(\omega t). \end{aligned} \quad (S4)$$

Rewriting (S4) as

$$\begin{aligned} \cos \theta \sin \theta \sin(\omega t) \cos(\omega t) &= \cos \theta \sin(\omega t) \sin(\omega t + \theta) \\ &\quad - \cos^2 \theta \sin^2(\omega t), \end{aligned} \quad (S5)$$

and substituting (S5) in (S3) yields

$$\begin{aligned} \sin^2(\omega t + \theta) &= (\cos^2 \theta - \sin^2 \theta) \sin^2(\omega t) \\ &\quad + \sin^2 \theta + 2 \cos \theta \sin(\omega t) \sin(\omega t + \theta) \\ &\quad - 2 \cos^2 \theta \sin^2(\omega t) \\ &= -\sin^2(\omega t) + 2 \cos \theta \sin(\omega t) \sin(\omega t + \theta) + \sin^2 \theta. \end{aligned} \quad (S6)$$

The input–output map of $\sin(\omega t)$ and $\sin(\omega t + \theta)$ is thus represented by

$$\begin{aligned} \sin^2(\omega t) - 2 \cos \theta \sin(\omega t) \sin(\omega t + \theta) \\ + \sin^2(\omega t + \theta) - \sin^2 \theta = 0, \end{aligned} \quad (S7)$$

which is an ellipse equation of the form

$$ax^2 + bxy + cy^2 + dx + fy + g = 0, \quad (S8)$$

where $x \triangleq \sin(\omega t)$, $y \triangleq \sin(\omega t + \theta)$, $a = c = 1$, $b = -2 \cos \theta$, $d = f = 0$, and $g = -\sin^2 \theta$. The eccentricity of (S8) is given by [S1]

$$e = \sqrt{\frac{2\sqrt{(a-c)^2 + b^2}}{\eta(a+c) + \sqrt{(a-c)^2 + b^2}}}, \quad (S9)$$

where

$$\begin{aligned} \eta &= -\text{sign} \det \begin{bmatrix} a & b/2 & d/2 \\ b/2 & c & f/2 \\ d/2 & f/2 & g \end{bmatrix} \\ &= -\text{sign} \det \begin{bmatrix} 1 & -\cos \theta & 0 \\ -\cos \theta & 1 & 0 \\ 0 & 0 & -\sin^2(\theta) \end{bmatrix} \\ &= -\text{sign}(-\sin^4 \theta) \\ &= 1. \end{aligned} \quad (S10)$$

Hence, (S9) implies that

$$e = \sqrt{\frac{2|\cos \theta|}{1 + |\cos \theta|}}. \quad (S11)$$

Therefore,

$$|\cos \theta| = \frac{e^2}{2 - e^2}. \quad (S12)$$

If the input–output map is a circle, then $e = 0$ and (S12) implies that $\theta = 90^\circ$ or $\theta = -90^\circ$. If the input–output map is a line segment, then $e = 1$ and (S12) implies that $\theta = 0^\circ$ or 180° .

REFERENCE

[S1] Eccentricity (mathematics). [Online]. Available: [http://en.wikipedia.org/wiki/Eccentricity_\(mathematics\)](http://en.wikipedia.org/wiki/Eccentricity_(mathematics))

where $|G(1j)| = 1/\sqrt{2}$ and $\angle G(1j) = -\pi/4$. Consider the state space realization of (9) given by

$$A = -1, B = 1, C = 1. \quad (11)$$

Figure 2 shows that $y - y_{\text{hss}}$ converges to zero for the nonzero initial condition $x(0) = 5$. Figure 3 shows that the amplification of y_{hss} relative to u is $|G(1j)| = 1/\sqrt{2}$, while the phase shift of y_{hss} relative to u is $\angle G(1j) = -45^\circ$. Figure 4 shows that the phase shift of y_{hss} relative to u

determines the slope of the semimajor axis of the ellipse, the eccentricity of the ellipse, and the orientation of the input–output map. ■

Example 2

Consider the semistable plant [4]

$$G(s) = \frac{1}{s(s+1)}, \quad (12)$$

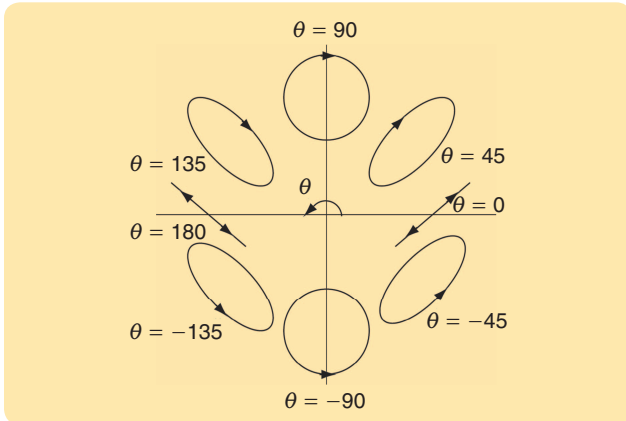


FIGURE 1 The relationship between the phase shift angle $\theta = \angle G(j\omega)$ in degrees and the input–output map for asymptotically stable linear systems, where the amplitude of the input and the output are normalized. The arrows indicate the orientation of the input–output maps.

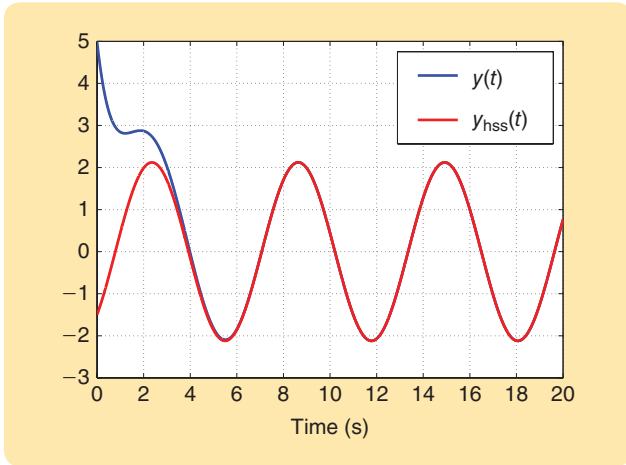


FIGURE 2 Output y and harmonic steady-state output y_{hss} for Example 1, where the plant (9) is asymptotically stable with the non-zero initial condition $x(0) = 5$. Note that y tends to y_{hss} .

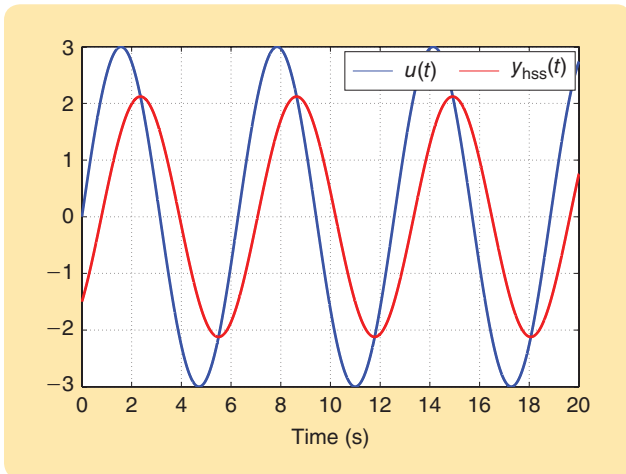


FIGURE 3 Input $u(t) = 3\sin(t)$ and harmonic steady-state output y_{hss} for Example 1, where the plant (9) is asymptotically stable. The amplification of y_{hss} relative to u is $|G(1j)| = 1/\sqrt{2}$, while the phase shift of y_{hss} relative to u is $\angle G(1j) = -45^\circ$.

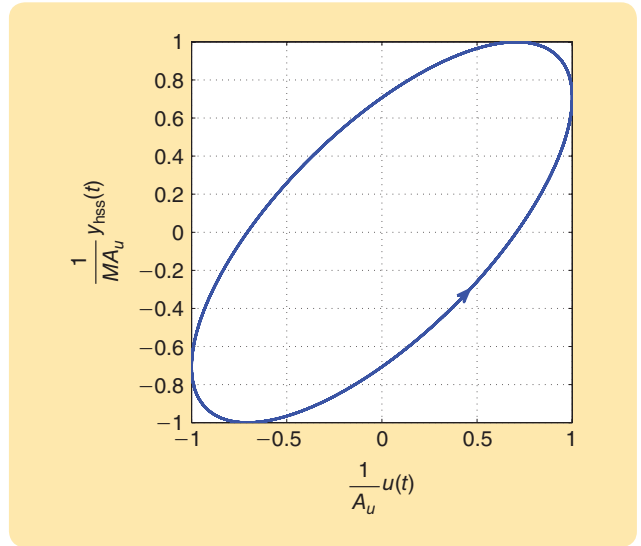


FIGURE 4 The normalized harmonic steady-state output $(1/MA_u)y_{\text{hss}}$ versus normalized input $(1/A_u)u$ for Example 1, where $M = \sqrt{2}$ and $A_u = 3$. This input–output map is an ellipse due to the fact that $(1/A_u)u$ and $(1/MA_u)y_{\text{hss}}$ are sinusoids with the same frequency. Note that the slope of the semimajor axis of the ellipse is one, and the orientation of the plot is counterclockwise, which indicates that the phase shift of y_{hss} relative to u is in $(-90, 0)^\circ$. The eccentricity of the ellipse is $e = \sqrt{2}/(1 + \sqrt{2})$. Therefore, (S12) implies that the phase shift of y_{hss} relative to u is -45° .

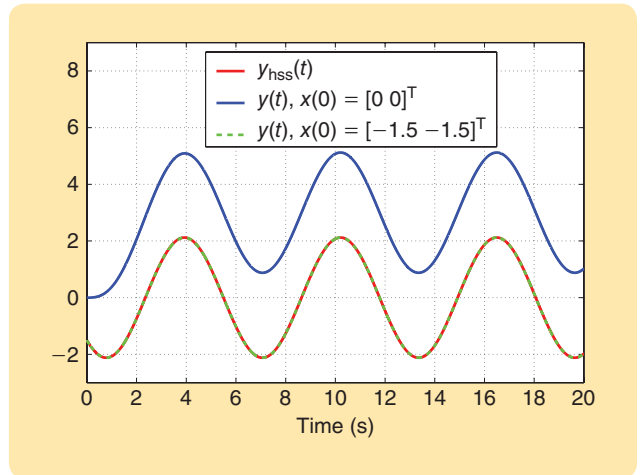


FIGURE 5 Output y and harmonic steady-state output y_{hss} for Example 2, where the plant (12) is semistable with zero initial conditions (solid blue). For this example, y does not tend to y_{hss} because (12) has a pole at the origin, which is responsible for the constant offset. Moreover, note that the output corresponding to the nonzero initial condition $x(0) = [-1.5 -1.5]^T$ (dashed green) is identical to y_{hss} .

with $u(t) = 3\sin(t)$ and $x(0) = 0$. Figure 5 shows that y_{trans} does not converge to zero with $x(0) = 0$ due to the transient component of y , which does not converge to zero. However, consider the state-space realization of (12) given by

$$A = \begin{bmatrix} -1 & 0 \\ 1 & 0 \end{bmatrix}, B = \begin{bmatrix} 1 \\ 0 \end{bmatrix}, C = [0 \ 1]. \quad (13)$$

Then, in accordance with (8), if $x(0) = [-1.5 \ -1.5]^T$, then $y_{\text{trans}}(t) = 0$ for all $t \geq 0$. Figure 6 shows that the amplification of y_{hss} relative to u is $|G(1j)| = 1/\sqrt{2}$, while the phase shift of y_{hss} relative to u is $\angle G(1j) = -135^\circ$. Figure 7 shows the input-output map of (12). ■

Example 3

Consider the Lyapunov-stable undamped oscillator

$$G(s) = \frac{1}{s^2 + 4}, \quad (14)$$

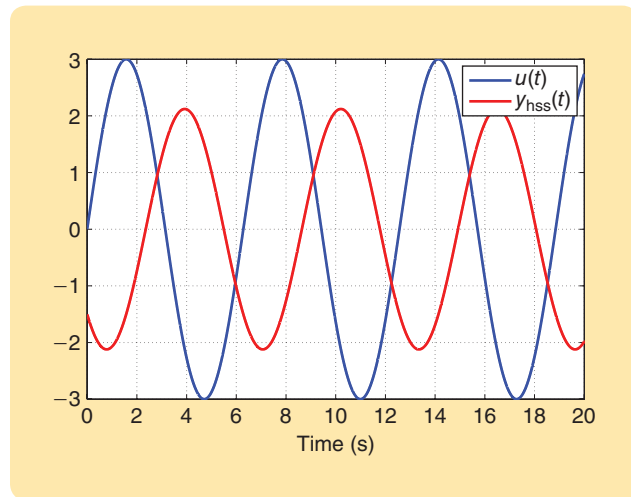


FIGURE 6 Input $u(t) = 3 \sin(t)$ and harmonic steady-state output y_{hss} for Example 2, where the plant (12) is semistable. The amplification of y_{hss} relative to u is $|G(1j)| = 1/\sqrt{2}$, while the phase shift of y_{hss} relative to u is $\angle G(1j) = -135^\circ$.

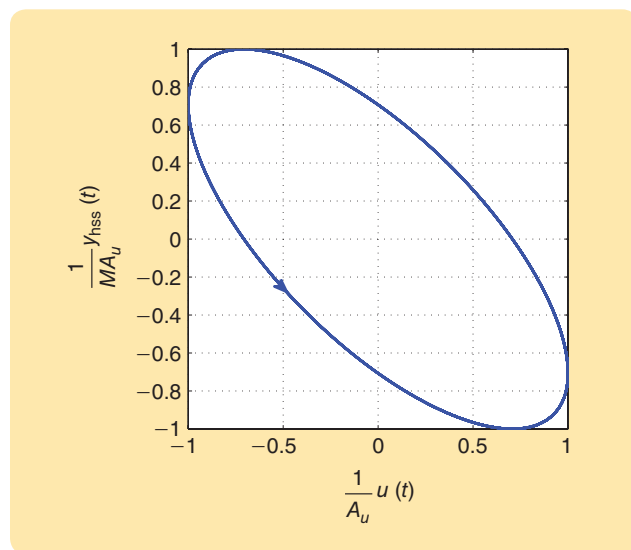


FIGURE 7 The normalized harmonic steady-state output $(1/MA_u)y_{\text{hss}}$ versus normalized input $(1/A_u)u$ for Example 2, where $M = 1/\sqrt{2}$ and $A_u = 3$. Note that the slope of the semimajor axis of the ellipse is -1 and the orientation of the plot is counterclockwise, which indicates that the phase shift of y_{hss} relative to u is in $(-180, -90)^\circ$. The eccentricity of the ellipse is $e = \sqrt{2}/(1 + \sqrt{2})$. Therefore, (S12) implies that the phase shift of y_{hss} relative to u is -135° .

with $u(t) = 3 \sin(t)$ and $x(0) = 0$. Figure 8 shows that $y - y_{\text{hss}}$ does not converge to zero due to the transient component of y , which does not converge to zero. Figure 9 shows that the amplification of y_{hss} relative to u is $|G(1j)| = 1/3$, while the phase shift of y_{hss} relative to u is $\angle G(1j) = 0$. Figure 10 shows the input-output map of (14). ■

Example 4

Consider the linearly unstable rigid-body plant

$$G(s) = \frac{1}{s^2}, \quad (15)$$

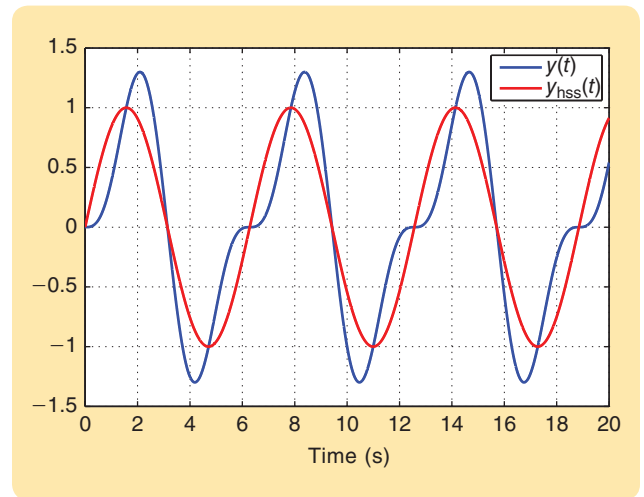


FIGURE 8 Output y and harmonic steady-state output y_{hss} for Example 3, where the plant (14) is Lyapunov stable with zero initial conditions. The plant has two poles at the imaginary axis and thus y does not tend to y_{hss} .

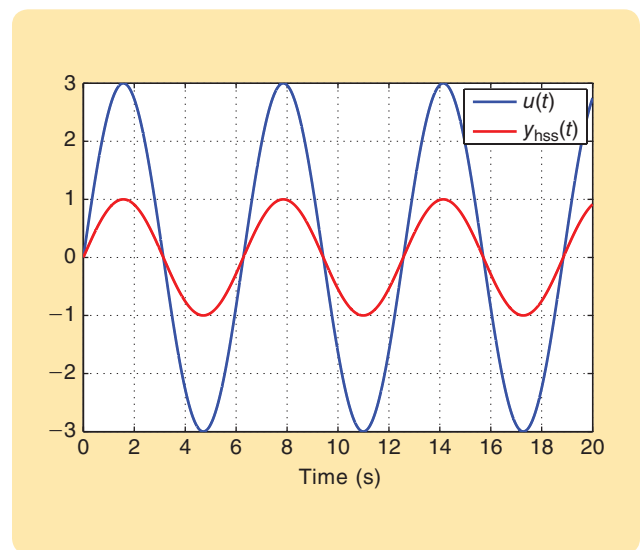


FIGURE 9 Input $u(t) = 3 \sin(t)$ and harmonic steady-state output y_{hss} for Example 3, where the plant (14) is Lyapunov stable. The amplification of y_{hss} relative to u is $|G(1j)| = 1/3$, while the phase shift of y_{hss} relative to u is $\angle G(1j) = 0^\circ$.

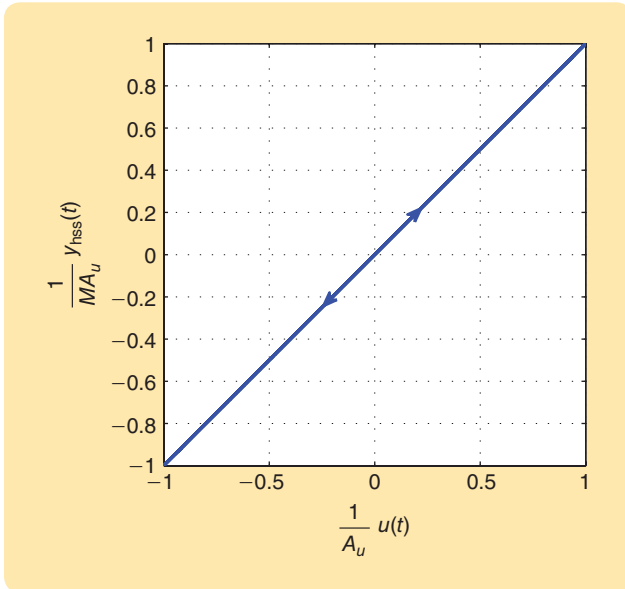


FIGURE 10 Normalized harmonic steady-state output $(1/MA_u)y_{\text{hss}}$ versus normalized input $(1/A_u)u$ for Example 3, where $M=1/3$ and $A_u=3$. This input–output map is a line segment due to the fact that u and y_{hss} are sinusoids with the same frequency and with zero relative phase shift.

with $u(t) = 3 \sin(t)$ and $x(0) = 0$. Figure 11 shows that $y - y_{\text{hss}}$ does not converge to zero due to the unbounded transient component of y , which does not converge to zero. Figure 12 shows that the amplification of y_{hss} relative to u is $|G(1j)| = 1$, while the phase shift of y_{hss} relative to u is $\angle G(1j) = 180^\circ$. Figure 13 shows the input–output map of (15). ■

Example 5

Consider the exponentially unstable plant

$$G(s) = \frac{2s+1}{(s+0.5)(s-1)}, \quad (16)$$

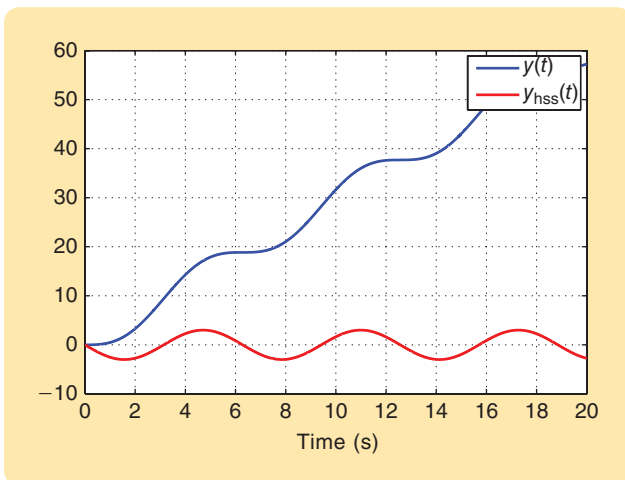


FIGURE 11 Output y and harmonic steady-state output y_{hss} for Example 4, where the plant (15) is linearly unstable with zero initial conditions. For this example, y does not tend to y_{hss} because the plant has two poles at the origin.

with $u(t) = 2 \sin(t)$ and $x(0) = 0$. Figure 14 shows that $y - y_{\text{hss}}$ does not converge to zero due to the unbounded transient component of y . ■

AMPLIFICATION AND PHASE SHIFT OF UNSTABLE SYSTEMS

Consider the block diagram in Figure 15, where C is the controller and the plant G is unstable. We assume that unstable pole-zero cancellation between C and G does not occur, and the closed-loop system is asymptotically stable. The command r is sinusoidal, e_r is the error, u is the control signal, and y is the output of the closed-loop system. Moreover, let $\hat{r}(s)$, $\hat{e}_r(s)$, $\hat{u}(s)$, and $\hat{y}(s)$ represent the Laplace transforms of r , e_r , u , and y , respectively.

Next, define the asymptotically stable transfer functions

$$L_{y,r}(s) \triangleq \frac{C(s)G(s)}{1+C(s)G(s)} = \frac{\hat{y}(s)}{\hat{r}(s)} \quad (17)$$

and

$$L_{u,r}(s) \triangleq \frac{C(s)}{1+C(s)G(s)} = \frac{\hat{u}(s)}{\hat{r}(s)}. \quad (18)$$

Letting $r(t) = A_r \sin(\omega t)$, Theorem 1 with (17) and (18) implies

$$y_{\text{hss}}(t) = A_r |L_{y,r}(j\omega)| \sin(\omega t + \angle L_{y,r}(j\omega)) \quad (19)$$

and

$$u_{\text{hss}}(t) = A_r |L_{u,r}(j\omega)| \sin(\omega t + \angle L_{u,r}(j\omega)). \quad (20)$$

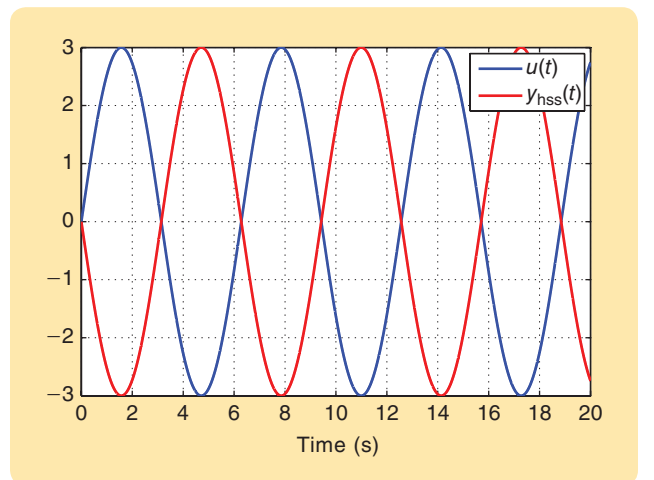


FIGURE 12 Input $u(t) = 3 \sin(t)$ and harmonic steady-state output y_{hss} for Example 4, where the plant (14) is linearly unstable. The amplification of y_{hss} relative to u is $|G(1j)| = 1$, while the phase shift of y_{hss} relative to u is $\angle G(1j) = 180^\circ$.

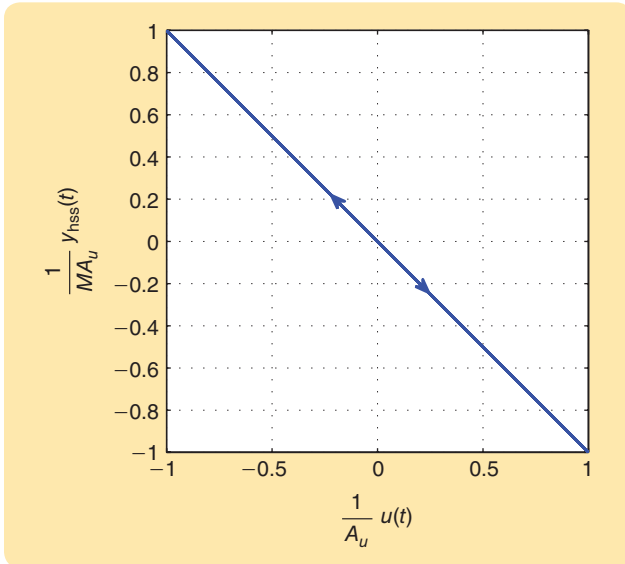


FIGURE 13 The normalized harmonic steady-state output $(1/MA_u)y_{\text{hss}}$ versus normalized input $(1/A_u)u$ for Example 4, where $M = 1$ and $A_u = 3$. This input–output map is a line segment due to the fact that u and y_{hss} are sinusoids with the same frequency and with 180° phase shift.

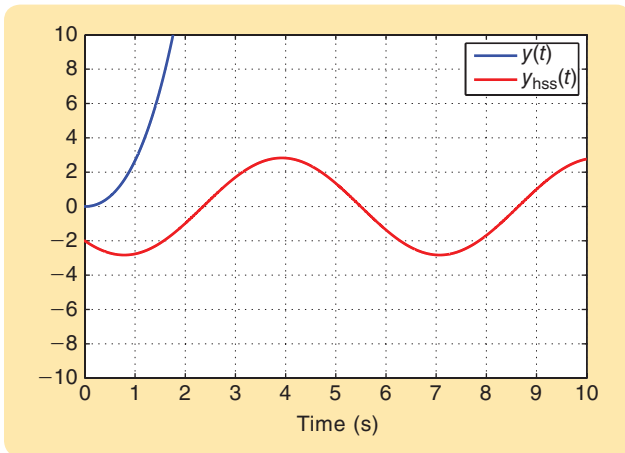


FIGURE 14 Output y and harmonic steady-state output y_{hss} for Example 5, where the plant (16) is exponentially unstable with zero initial conditions. For this example, y does not tend to y_{hss} because (16) has an unstable pole.

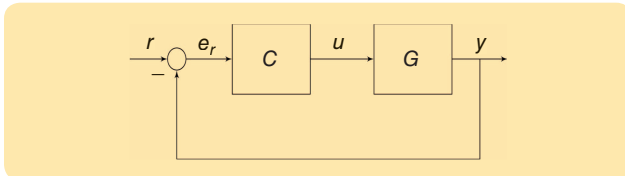


FIGURE 15 A closed-loop control system with controller C and plant G . The G is unstable, and the closed-loop system is assumed to be asymptotically stable.

Letting $\mathcal{A}(y_{\text{hss}})$ and $\mathcal{A}(u_{\text{hss}})$ denote the amplitudes of y_{hss} and u_{hss} , respectively, it follows from (19) and (20) that

$$\mathcal{A}(y_{\text{hss}}) = A_r |L_{y,r}(j\omega)|, \quad (21)$$

$$\mathcal{A}(u_{\text{hss}}) = A_r |L_{u,r}(j\omega)|. \quad (22)$$

Dividing (21) by (22) and using (17) and (18) yields, for all $\omega \in \mathbb{R}$,

$$\begin{aligned} \frac{\mathcal{A}(y_{\text{hss}})}{\mathcal{A}(u_{\text{hss}})} &= \frac{A_r |L_{y,r}(j\omega)|}{A_r |L_{u,r}(j\omega)|} \\ &= \frac{|C(j\omega)G(j\omega)|}{|1 + C(j\omega)G(j\omega)|} \\ &= \frac{|C(j\omega)|}{|1 + C(j\omega)G(j\omega)|} \\ &= |G(j\omega)|, \end{aligned} \quad (23)$$

which shows that $|G(j\omega)|$ is the amplification of y_{hss} relative to u_{hss} . Moreover, it follows from (19) and (20) that the phase shift of y_{hss} relative to u_{hss} is

$$\begin{aligned} \angle L_{y,r}(j\omega) - \angle L_{u,r}(j\omega) &= \angle C(j\omega)G(j\omega) \\ &\quad - \angle(1 + C(j\omega)G(j\omega)) \\ &= [\angle C(j\omega) \\ &\quad - \angle(1 + C(j\omega)G(j\omega))] \\ &= \angle G(j\omega). \end{aligned} \quad (24)$$

The amplification and phase shift of the plant are properties of the plant and are independent of the controller and the rate of convergence to harmonic steady state.

Example 6

Consider the exponentially unstable transfer function

$$G(s) = \frac{2s + 1}{(s + 0.5)(s - 1)} \quad (25)$$

with the lead controller

$$C(s) = \frac{s + 8}{s + 10} \quad (26)$$

and the command $r(t) = 2 \sin(t)$. It follows that

$$L_{y,r}(s) = \frac{2s + 16}{s^2 + 11s + 6} \quad (27)$$

and

$$L_{u,r}(s) = \frac{s^2 + 7s - 8}{s^2 + 11s + 6} \quad (28)$$

are asymptotically stable. Consider the state-space realization of (27) given by

$$\begin{aligned} A &= \begin{bmatrix} -11 & -6 \\ 1 & 0 \end{bmatrix}, \quad B = \begin{bmatrix} 1 \\ 0 \end{bmatrix} \\ C &= [2 \quad 16], \quad D = 0. \end{aligned} \quad (29)$$

Figure 16 shows that $y - y_{\text{hss}}$ converges to zero for the asymptotically stable plant (27) with the nonzero initial

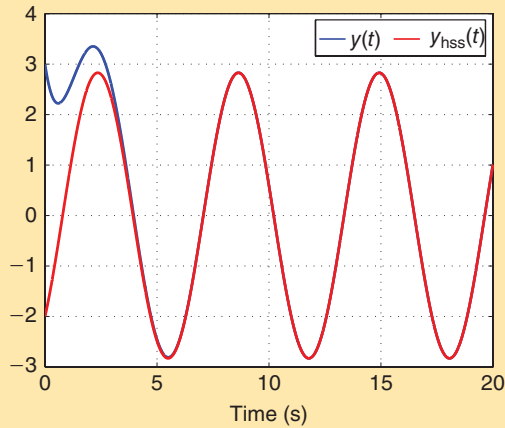


FIGURE 16 Output y and harmonic steady-state output y_{hss} for the asymptotically stable closed-loop transfer function (27) in Example 6 with the realization (29) and nonzero initial condition $x(0) = [0.5 \ 0.1]^T$. Note that, since (27) is asymptotically stable, y tends to y_{hss} .

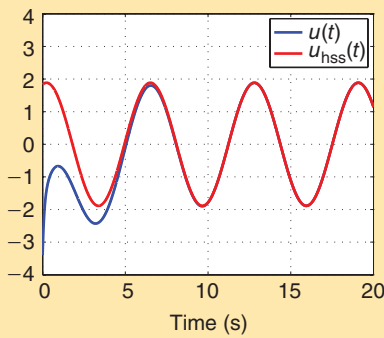


FIGURE 17 Input u and harmonic steady-state input u_{hss} given by the asymptotically stable closed-loop transfer function (28) in Example 6 with the realization (30) and nonzero initial condition $x(0) = [0.5 \ 0.1]^T$. Note that, since (28) is asymptotically stable, u tends to u_{hss} .

condition $x(0) = [0.5 \ 0.1]^T$. Consider the state-space realization of (28) given by

$$\begin{aligned} A &= \begin{bmatrix} -11 & -6 \\ 1 & 0 \end{bmatrix}, & B &= \begin{bmatrix} 1 \\ 0 \end{bmatrix}, \\ C &= [-4 \ -14], & D &= 1. \end{aligned} \quad (30)$$

Figure 17 shows that $u - u_{\text{hss}}$ converges to zero for the asymptotically stable plant (28) with the nonzero initial condition $x(0) = [0.5 \ 0.1]^T$. Figure 18 shows that the amplification of y_{hss} relative to u_{hss} is $|G(1j)| = \sqrt{2}$, while the phase shift of y_{hss} relative to u_{hss} is $\angle G(1j) = -135^\circ$. The input–output map of (25) is shown in Figure 19, and the Bode plots of (25) and (26) are in Figure 20. Note from Figure 20 that $|G(1j)| = \sqrt{2}$ and $\angle G(1j) = -135^\circ$. Figure 21 shows the Bode plot of the closed-loop transfer function (27). Both the frequency response of the un-

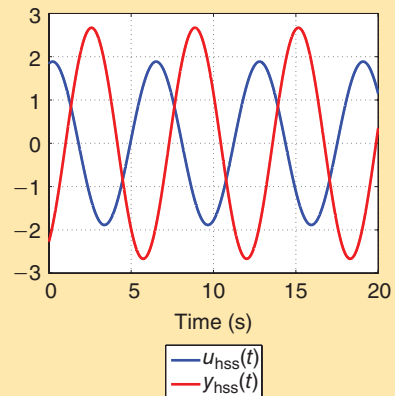


FIGURE 18 Harmonic steady-state input u_{hss} and harmonic steady-state output y_{hss} for Example 6. The amplification of y_{hss} relative to u_{hss} is $|G(1j)| = \sqrt{2}$, while the phase shift of y_{hss} relative to u_{hss} is $\angle G(1j) = -135^\circ$.

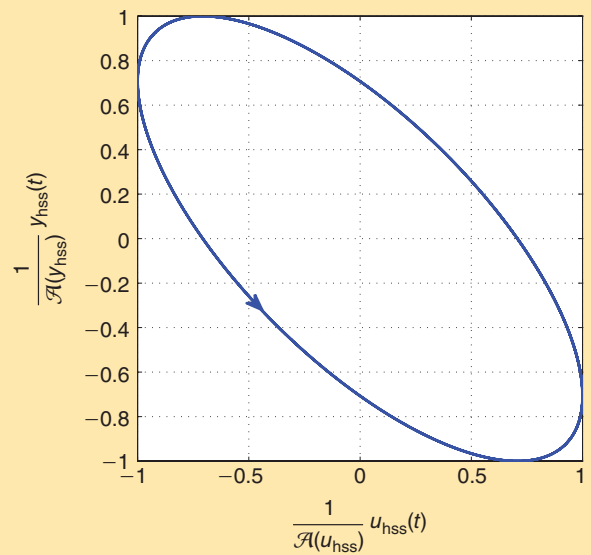


FIGURE 19 The normalized harmonic steady-state output $1/(\mathcal{A}(y_{\text{hss}}))y_{\text{hss}}$ versus the normalized harmonic steady-state input $1/(\mathcal{A}(u_{\text{hss}}))u_{\text{hss}}$ for Example 6, where $\mathcal{A}(y_{\text{hss}}) \approx 1.8872$ and $\mathcal{A}(u_{\text{hss}}) \approx 2.6689$. This input–output map is an ellipse due to the fact that u_{hss} and y_{hss} are sinusoids with the same frequency. Note that the slope of the semimajor axis of the ellipse is -1 , and the orientation of the plot is counterclockwise, which indicates that the phase shift of y_{hss} relative to u is in $(-180, -90)^\circ$. The eccentricity of the ellipse is $e = \sqrt{2}/(1 + \sqrt{2})$. Therefore, (S12) implies that the phase shift of y_{hss} relative to u is -135° .

stable plant and the frequency response of the controller shown in Figure 20 contribute to the frequency response of the closed-loop transfer function (27). In particular, (17) indicates that $|L_{y,r}(j\omega)| = (|C(j\omega)| |G(j\omega)|) / (|1 + C(j\omega)G(j\omega)|)$ and $\angle L_{y,r}(j\omega) = \angle C(j\omega) + \angle G(j\omega) - \angle(1 + C(j\omega)G(j\omega))$. ■

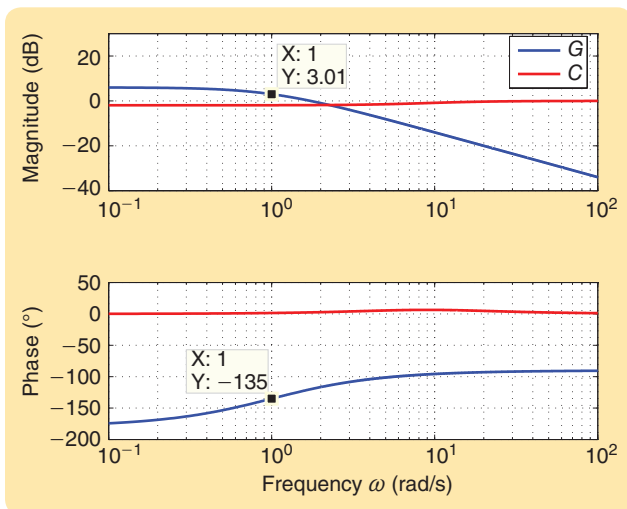


FIGURE 20 Bode plots for (25) and (26) in Example 6. The amplification of y_{hss} relative to u_{hss} at $\omega = 1$ rad/s, both of which are shown in Figure 18, is $|G(1j)| = \sqrt{2}$, which is approximately 3.01 dB as shown by the magnitude Bode plot. Moreover, the phase shift of y_{hss} relative to u_{hss} at $\omega = 1$ rad/s, both of which are shown in Figure 18, is $\angle G(1j) = -135^\circ$ as shown by the phase Bode plot.

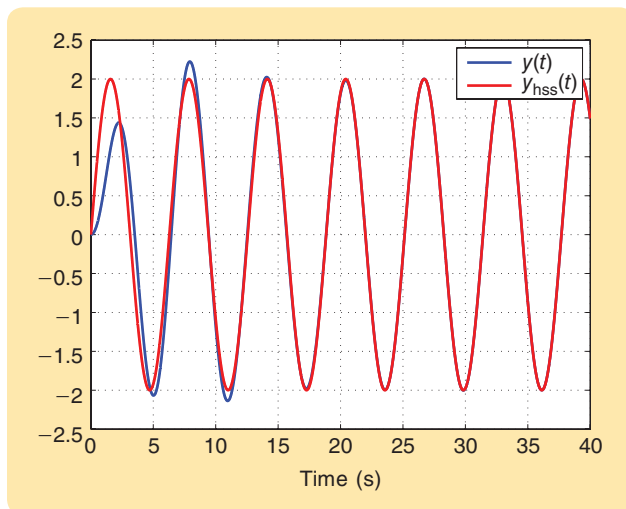


FIGURE 22 Output y and harmonic steady-state output y_{hss} for the asymptotically stable transfer function (32) in Example 7, where the initial conditions of the plant and the controller are zero. Note that, since (32) is asymptotically stable, y tends to y_{hss} .

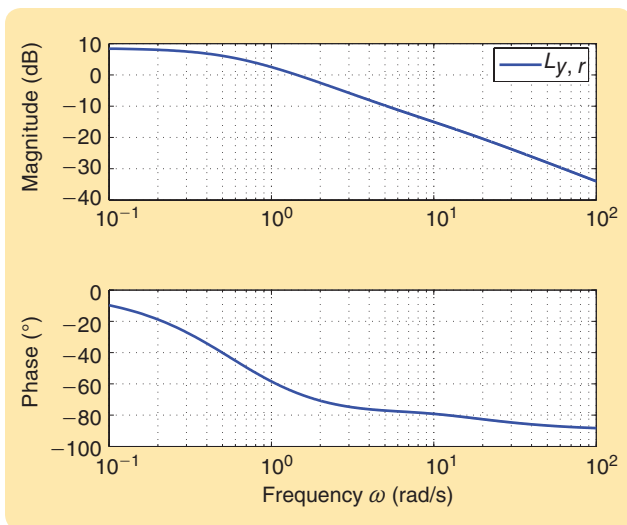


FIGURE 21 A Bode plot for the closed-loop transfer function (27) in Example 6. The frequency response of the unstable plant and the frequency response of the controller, both of which are shown in Figure 20, contribute to the frequency response of the closed-loop transfer function (27). In particular, (17) indicates that $|L_{y,r}(j\omega)| = (|C(j\omega)||G(j\omega)|)/|1 + C(j\omega)G(j\omega)|$ and $\angle L_{y,r}(j\omega) = \angle C(j\omega) + \angle G(j\omega) - \angle(1 + C(j\omega)G(j\omega))$.

Example 7

Consider the linearly unstable rigid-body plant (15) with proportion-integral-derivative controller

$$C(s) = 2 + \frac{1}{s} + s \quad (31)$$

and the command $r(t) = \sin(t)$. It follows that

$$L_{y,r}(s) = \frac{s^2 + 2s + 1}{s^3 + s^2 + 2s + 1} \quad (32)$$

and

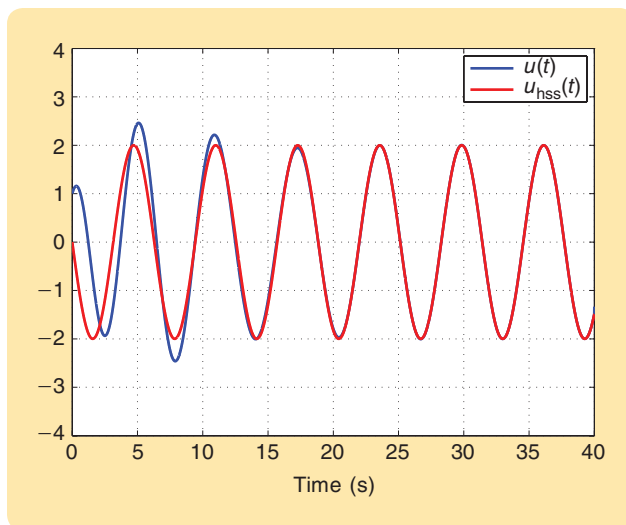


FIGURE 23 Input u and harmonic steady-state input u_{hss} given by the asymptotically stable transfer function (33) in Example 7, where the initial conditions of the plant and the controller are zero. Note that, since (33) is asymptotically stable, u tends to u_{hss} .

$$L_{u,r}(s) = \frac{s^2(s^2 + 2s + 1)}{s^3 + s^2 + 2s + 1} \quad (33)$$

are asymptotically stable. Figure 22 shows that $y - y_{\text{hss}}$ converges to zero for the asymptotically stable transfer function (32) where the initial conditions of the plant and the controller are zero. Figure 23 shows that $u - u_{\text{hss}}$ converges to zero for the asymptotically stable transfer function (33) where the initial conditions of the plant and the controller are zero.

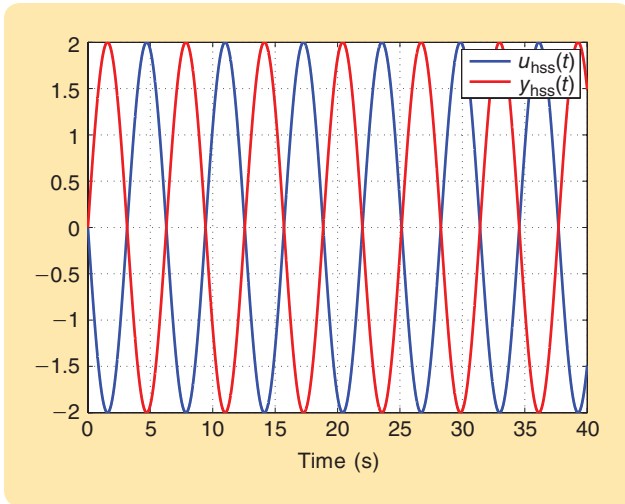


FIGURE 24 The harmonic steady-state input u_{hss} and the harmonic steady-state output y_{hss} for Example 7. The amplification of y_{hss} relative to u_{hss} is $|G(1j)| = 1$, while the phase shift of y_{hss} relative to u_{hss} is $\angle G(1j) = 180^\circ$.

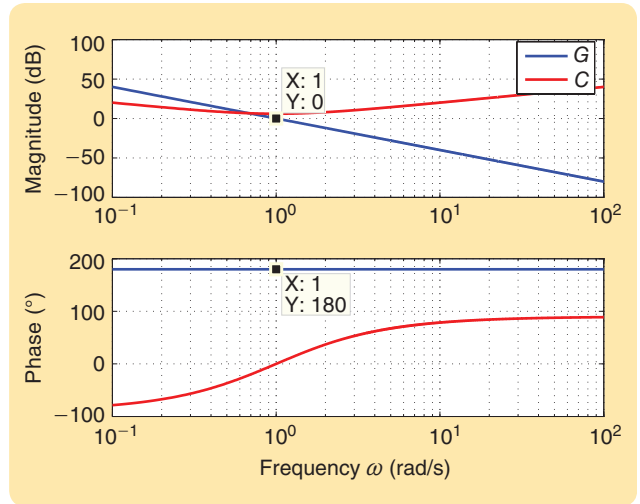


FIGURE 26 Bode plots for (15) and (31) in Example 7. The amplification of y_{hss} relative to u_{hss} at $\omega = 1$ rad/s, both of which are shown in Figure 24, is $|G(1j)| = 1$, which is equivalent to 0 dB as shown by the magnitude Bode plot. Moreover, the phase shift of y_{hss} relative to u_{hss} at $\omega = 1$ rad/s, both of which are shown in Figure 18, is $\angle G(1j) = 180^\circ$ as shown by the phase Bode plot.

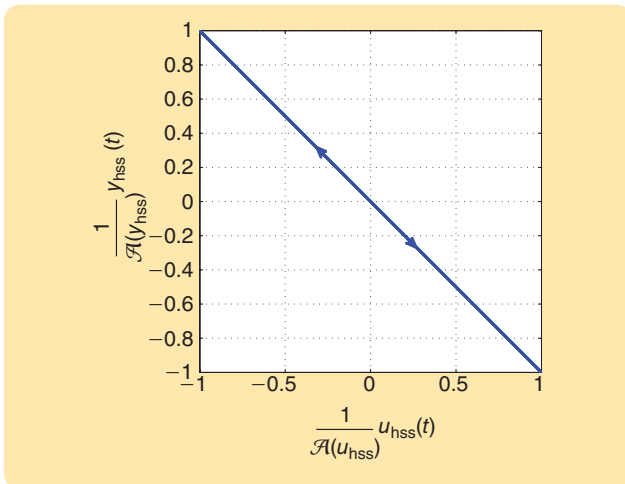


FIGURE 25 The normalized harmonic steady-state output $1/(\mathcal{A}(y_{\text{hss}}))y_{\text{hss}}$ versus the normalized harmonic steady-state input $1/(\mathcal{A}(u_{\text{hss}}))u_{\text{hss}}$ for Example 7, where $\mathcal{A}(y_{\text{hss}}) = 2$ and $\mathcal{A}(u_{\text{hss}}) = 2$. This input–output map is a line segment due to the fact that u_{hss} and y_{hss} are sinusoids with the same frequency and 180° phase shift.

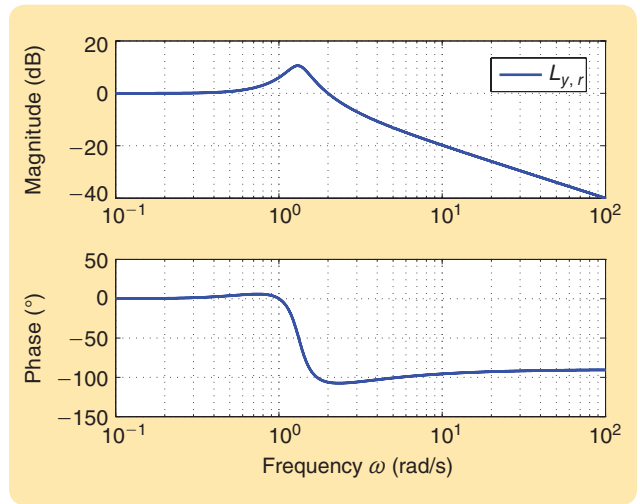


FIGURE 27 The Bode plot for the closed-loop transfer function (32) in Example 7. The frequency response of the unstable plant and the frequency response of the controller, both of which are shown in Figure 26, contribute to the frequency response of the closed-loop transfer function (32). In particular, (17) indicates that $|L_{y,r}(j\omega)| = (|C(j\omega)| |G(j\omega)|) / (|1 + C(j\omega)G(j\omega)|)$ and $\angle L_{y,r}(j\omega) = \angle C(j\omega) + \angle G(j\omega) - \angle(1 + C(j\omega)G(j\omega))$.

Figure 24 shows that the amplification of y_{hss} relative to u_{hss} is $|G(1j)| = 1$, while the phase shift of y_{hss} relative to u_{hss} is $\angle G(1j) = 180^\circ$. The input–output map of (15) is shown in Figure 25 and the Bode plots of (15) and (31) in Figure 26. Note from Figure 26 that $|G(1j)| = 1$ and $\angle G(1j) = 180^\circ$. Figure 27 shows the Bode plot of the closed-loop transfer function (32). Both the frequency response of the unstable plant and the frequency response of the controller shown in Figure 26 contribute to the frequency response of the closed-loop transfer function (32). In particular, (17) indicates that $|L_{y,r}(j\omega)| = (|C(j\omega)| |G(j\omega)|) / (|1 + C(j\omega)G(j\omega)|)$ and $\angle L_{y,r}(j\omega) = \angle C(j\omega) + \angle G(j\omega) - \angle(1 + C(j\omega)G(j\omega))$. ■

AUTHOR INFORMATION

Khaled F. Aljanaideh received the B.Sc. degree in mechanical engineering from Jordan University of Science and Technology, Irbid, Jordan, in 2009 and the M.S.E. degree in aerospace engineering from the University of Michigan, Ann Arbor, in 2011, where he is currently working toward the Ph.D. degree. His research interests include system identification and adaptive control.

(continued on page 141)

» 2017

- ▲ **IEEE CONFERENCE ON CONTROL TECHNOLOGY AND APPLICATIONS (CCTA 2017)**
TBD 2017
TBD
General Chair: Stephen Yurkovich
Program Chairs: Mark W. Spong and Mario A. Rotea
- ▲ **AMERICAN CONTROL CONFERENCE (ACC 2017)**
24–25 May
Seattle, Washington, USA
General Chair: Jing Sun
Program Chair: Rajesh Rajamani
- ▲ **IEEE CONFERENCE ON DECISION AND CONTROL (CDC 2017)**
December
TBD
General Chairs: Richard H. Middleton and Dragan Nesic

» 2018

- ▲ **AMERICAN CONTROL CONFERENCE (ACC 2018)**
27–29 June
Milwaukee, Wisconsin, USA
General Chair: Jordan M. Berg
Program Chair: Zongli Lin
- ▲ **IEEE CONFERENCE ON CONTROL TECHNOLOGY AND APPLICATIONS (CCTA 2018)**
TBD 2018
TBD
General Chair: Jakob Stoustrup

We want to hear from you!

Do you like what you're reading?

Let us know—send an e-mail to the Editor-in-Chief.

Letters may be published in future issues and edited for style.

» **LECTURE NOTES** (continued from page 95)

James R. Forbes received the B.A.Sc. in mechanical engineering (honors, co-op) from the University of Waterloo in 2006. He received the M.A.Sc. and Ph.D. degrees in aerospace science and engineering from the University of Toronto Institute for Aerospace Studies in 2008 and 2011, respectively. From May 2011 to August 2013, he was an assistant professor of mechanical engineering at McGill University, Montreal, Quebec, Canada. While at McGill University, he was also an associate member of the Centre for Intelligent Machines. He is currently an assistant professor of aerospace engineering at the University of Michigan. The focus of his research is the dynamics and control of robotic and aerospace systems.

Dennis S. Bernstein is a professor in the Aerospace Engineering Depart-

ment at the University of Michigan. His interests are in identification and adaptive control for aerospace applications.

REFERENCES

- [1] G. F. Franklin, J. D. Powell, and A. Emami-Naeini, *Feedback Control of Dynamic Systems*. Upper Saddle River, NJ: Prentice Hall, 2002.
- [2] D. S. Bernstein, *Matrix Mathematics: Theory, Facts, and Formulas*. Princeton, NJ: Princeton University Press, 2009.

- [3] Lissajous curve. [Online]. Available: http://en.wikipedia.org/wiki/Lissajous_curve
- [4] D. S. Bernstein and S. P. Bhat, "Lyapunov stability, semistability, and asymptotic stability of matrix second-order systems," *J. Mech. Des.*, vol. 117, no. B, pp. 145–153, 1995.

The goal of this article is to investigate whether or not an unstable plant in a stabilized closed loop has amplification and phase shift in the sense of the harmonic steady-state response of an asymptotically stable system.

